Comparison of Wave Load Effects on a TLP Wind Turbine by Using Computational Fluid Dynamics and Potential Flow Theory Approaches

Ali Nematbakhsh[a,*], Erin E. Bachynski[a,b], Zhen Gao[a,b], Torgeir Moan[a,b]

[a] *Centre for Ships and Ocean Structures, Norwegian University of Science and Technology, NO-7491, Trondheim, Norway*
[b] *Centre for Autonomous Marine Operations and Systems, Norwegian University of Science and Technology, NO-7491, Trondheim, Norway*

Abstract

Tension Leg Platform (TLP) is one of the concepts which shows promising results during initial studies to carry floating wind turbines. One of the concerns regarding tension leg platform wind turbines (TLPWTs) is the high natural frequencies of the structure that may be excited by nonlinear waves loads. Since Computational Fluid Dynamics (CFD) models are capable of capturing nonlinear wave loads, they can lead to better insight about this concern. In the current study, a CFD model based on immersed boundary method, in combination with a two-body structural model of TLPWT is developed to study wave induced responses of TLPWT in deep water. The results are compared with the results of a potential flow theory-finite element software, SIMO-RIFLEX (SR). First, the CFD based model is described and the potential flow theory based model is briefly introduced. Then, a grid sensitivity study is performed and free decay tests are simulated to determine the natural frequencies of different motion modes of the TLPWT. The responses of the TLPWT to regular waves are studied, and the effects of wave height are investigated. For the studied wave heights which vary from small to medium amplitude (wave height over wavelength less than 0.071), the results predicted by the CFD based model are generally in good agreement with the potential flow theory based model. The only considerable difference is the TLPWT mean surge motion which is predicted higher by the CFD model, possibly because of considering the nonlinear effects of the waves loads and applying these loads at the TLPWT instantaneous position in the CFD model. This difference does not considerably affect the important TLPWT design driving parameters such as tendons forces and tower base moment, since it only affects the mean dynamic position of TLPWT. In the current study, the incoming wave frequency is set such that third-harmonic wave frequency coincides with the first tower bending mode frequency. However, for the studied wave conditions a significant excitation of tower natural frequency is not observed. The high stiffness of tendons which results in linear pitch motion of TLPWT hull (less than 0.02 degrees) and tower (less than 0.25 degrees) can explain the limited excitement of the tower first bending mode. The good agreement between CFD and potential flow theory based results for small and medium amplitude waves gives confidence to the proposed CFD based model to be further used for hydrodynamic analysis of floating wind turbines in extreme ocean conditions.

Keywords: Floating wind turbine, Tension leg platform, Computational fluid dynamics, Potential flow theory, Offshore structure

1. Introduction

Wind energy is one of the best options to produce renewable energy. Although land-based wind turbines are well developed, the offshore wind industry is still in development. Currently only 2% of the electricity, produced from wind resources, comes from offshore [1]. The main problem regarding harvesting energy from offshore wind turbines is the total cost of energy, which can be reduced if lighter support structures can be designed to carry offshore wind turbines. Lighter support structure design requires more reliable and precise analysis of the environmental loads.

TLP is one of the support structures which remains stable mainly through the mooring system which includes a number of pre-tensioned stiff tendons. The TLP concept was introduced in 1970s [2] for the oil and gas industry and has been built and used successfully afterwards, however there have always been concerns about nonlinear wave loads on TLPs. These nonlinear wave loads might excite the natural frequencies of the TLPs. Different experimental tests such as the experiments performed by Mercier et al. [3] and Lonergan et al. [4] showed the importance of this high order wave loads on TLPs. Later Faltinsen et al. [5] developed a formula (known as FNV formula), based on potential flow theory, to calculate some components of nonlinear wave loads on slender vertical cylinders. Their calculations and derived formula showed the importance of the third-order wave loads when the wave amplitude is of the same order as the cylinder diameter. For TLP structures these third-order wave loads are important since they might coincide with one of the structure's natural frequencies and can lead to transient large amplitude response of the structure (known as ringing) [6].

Initial analysis of TLP platforms to carry wind turbines also shows promising results [7, 8]. TLP platforms are very favourable to carry wind turbines because of very small pitch motion, leading to small nacelle motion. However, just as for TLPs designed for the oil and gas industry, TLPWT natural frequencies may be excited by the nonlinear wave loads. The linear hydrodynamic analysis of TLPWT has been studied extensively [9, 10, 11]. However, nonlinear models have only been used recently. Roald et al. [12] studied the effect of second-order wave loads on a TLP wind turbine and showed that including the sum-frequency second-order wave loads have considerable effects on the heave response of TLP wind turbine. Bae and Kim [13] studied the sum-frequency second-order wave loads on a TLP wind turbine. Their results for the considered 5 MW TLPWT showed that considering the sum-frequency wave loads may excite the TLPWT pitch natural frequency in the survival condition. Bachynski and Moan [14] studied the third-order loads on a TLPWT using the FNV formula. Their results indicated that, ringing has a considerable effect on the responses of TLPWTs which have natural pitch/bending periods around 3-4 seconds.

All of the mentioned nonlinear hydrodynamic load investigations are based on potential flow theory analysis which limits the hydrodynamic modeling to linear or weakly nonlinear models. Another approach is to use CFD methods which can model nonlinear wave loads very well. The CFD based models to simulate floating wind turbines are very recent. Beyer et al. [15] studied surge free decay test of a floating wind turbine by coupling a CFD model with FAST

*Corresponding author
Email address: ali.nematbakhsh@ntnu.no (Ali Nematbakhsh)

[16], a wind turbine design tool. They intended to obtain the damping coefficient of a floating wind turbine by using a CFD approach. Ren et al. [17] used a CFD based commercial software to simulate wind and wave loading on a TLPWT, however their model was only allowed to have surge motion, hence heave and pitch natural frequencies could not be excited. Benitz et al. [18] used OpenFOAM, an open source CFD based code, to study the wave loads on a semi-submersible wind turbine and compared the results with HydroDyn, a potential flow theory based code for hydrodynamic analysis [16]. A good agreement between two results was achieved, however in the simulations the effects of semi-submersible motions on the hydrodynamic loads were neglected. Finally, Liu and Hu [19] and Hu et al. [20] carried out CFD based analysis of different types of semi-submersible floating wind turbines with focus on hydrodynamic loads. They used CIP method [21] for the CFD simulations and compared their results with experimental data and achieved good agreement.

In order to better understand the nonlinear wave loads on TLPWTs, a CFD model in combination with multi-body approach for modeling a TLPWT is presented here and is used to study the interaction of this floating wind turbine with regular waves. Based on the presented model, the tower base bending moment due to the wave loading can also be investigated. All of the numerical results are compared with a potential flow theory-finite element software, SR. By using this CFD approach, the platform is completely free to float, linear assumption for the incoming wave is not required, and nearly all the nonlinear wave loads on the TLPWT can be captured without relying on any experimental coefficients. The current CFD model was initially proposed by Nematbakhsh et al. [22] and used to simulate a single rigid body TLP and a spar buoy floating wind turbine [23]. The numerical model was extended in Nematbakhsh et al. [24] to a two-body model and initial comparisons with potential flow theory approach results were performed for a modified TLPWT which has very stiff tendons and pitch motion was extremely small. The present research significantly extends the previous works [22, 23, 24] by improving the structural model of the TLPWT in which the tower and tendons damping effects are also considered, by presenting a more complete description of the two-body model of TLPWT, and by studying the responses of a TLPWT, designed by Bachynski et al. [11] for regular waves. In comparison of the results calculated by the CFD and potential flow theory approaches, in general good agreement between both models is obtained, although some limited differences in nonlinear components of the TLPWT responses are observed which will be discussed.

The rest of the paper is organized as follows. In section 2, the CFD based model and potential flow theory based software, SR, are described. In section 3, initially TLPWT free decay tests are performed and natural frequencies of the TLPWT are assessed. Then the responses of the TLPWT to incoming wave which has a chance of exciting the tower first bending mode are examined, and finally the effects of varying wave amplitudes on the TLPWT responses are studied. Conclusions are presented in section 4.

2. Computational Model

In this section the CFD based model which is the main focus of the current work is described in detail and a brief review of the potential flow theory based model is given.

2.1. CFD Based Model

The numerical model consists of a fluid-structure interaction part and a structural part. The fluid-structure part is developed based on solving Navier-Stokes equations. The structural part consists of the models used to simulate components of the floating wind turbine namely, the tendons, tower, rotor and the nacelle. These two parts are coupled and information is exchanged between these two parts at every time step. In the present work, NREL 5 *MW* wind turbine [25] is mounted on a TLP. The TLPWT is shown in Figure 1 and the properties are described in Table 1.

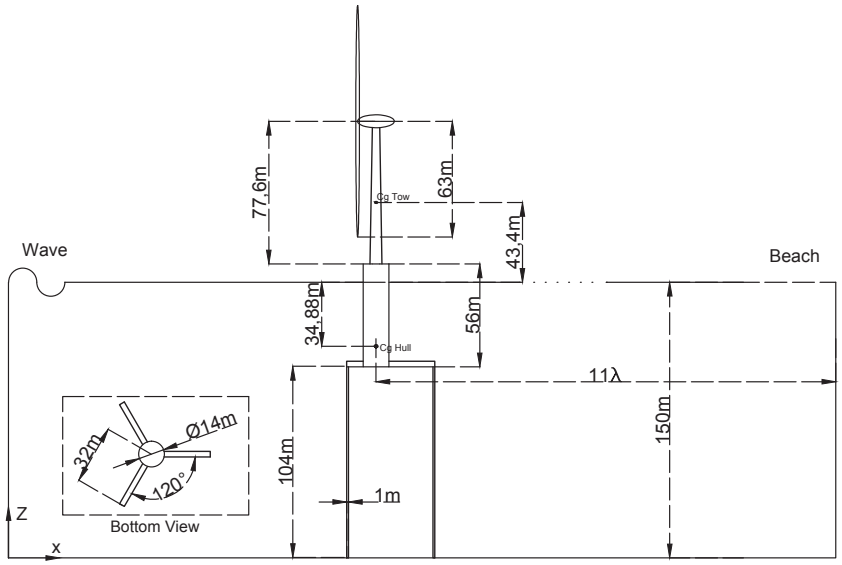

Figure 1: Sketch of the studied tension leg platform floating wind turbine (TLPWT)

2.1.1. Fluid-Structure Interaction Model

This part consists of solving the Navier-Stokes equations to follow the fluids' motion (water and air), tracking the free surface by using the level set method, modeling the floating wind turbine hull which interacts with water by an immersed boundary method, and finally determining a forcing term which couples this part with the structural part. This part has been verified in the works by Nematbakhsh et al. [22, 24, 26] by performing different numerical tests including; studying vortex shedding behind a circular cylinder and comparing the results with experimental data, comparing wave induced surge, heave and pitch responses of a barge with experimental data, and comparing hydrodynamic loads on a surface piercing fixed cylinder with experimental data.

Table 1: Properties of the studied tension leg platform wind turbine (TLPWT)

Hull mass (including ballast and not tower, rotor and nacelle)	4622 *tonnes*
Hull displacement	7258 *tonnes*
Hull center of buoyancy	-23 *m* respect to MWL
Hull mass moment of inertia respect to hull C_g	$I_{yy} = 0.658 \times 10^6$ *tonnes.m*^{2}
Tendon diameter, thickness and modulus of elasticity	1.00 *m*, 0.033 *m* & 210 *GPa*
Wind Turbine (Tower, Rotor, and Nacelle)	NREL 5 *MW*
Tower mass and moment of inertia respect to tower C_g	250 *tonnes* & $I_{yy} = 0.126 \times 10^6$ *tonnes.m*^{2}
Tower diameter, thickness and modulus of elasticity	5.185 *m*, 0.023 *m* & 210 *GPa*
Nacelle mass	240 *tonnes*
Rotor mass and moment of inertia respect to rotor C_g	110 *tonnes* & $I_{yy} = 0.915 \times 10^6$ *tonnes.m*^{2}

The Navier-Stokes equations which are supplemented by the continuity equation can be written as follows for incompressible flows;

$$\rho\left(\frac{\partial \mathbf{u}}{\partial t} + \nabla \cdot (\mathbf{uu})\right) = -\nabla p + \rho \mathbf{g} + \nabla \cdot \mu(\nabla \mathbf{u} + \nabla \mathbf{u}^T) + \mathbf{F} \tag{1}$$

$$\nabla \cdot \mathbf{u} = 0, \tag{2}$$

where ρ is density, $\mathbf{u}$ is velocity, $\mathbf{g}$ is the acceleration due to gravity, and μ is the dynamic viscosity. Equation 1 and Equation 2 are the standard equations to model incompressible fluids. There is only a force term $\mathbf{F}$ added to the right hand side of Equation 1. This term couples the fluid-structure part with the structural part and will be discussed at the end of Structural Model subsection.

The Navier-Stokes equations are solved in the whole domain including the water, the air and the solid by using second-order finite volume discretization methods in space and time. The advection terms are discretized by second-order ENO (essentially non-oscillatory) method [27], the viscous terms by a second-order central difference approach, the pressure is obtained by an iterative approach, and finally the velocities are updated by a second-order predictor-corrector method.

The updated velocities, obtained from the Navier-Stokes equations, are used to track the free surface of the waves. The free surface is in fact an air-water interface, hence one of the standard methods to model two-phase flows can be used [28]. The level set method [29, 30] is adopted which is a popular approach in two-phase flows simulations and can easily capture the interface between fluids with high density ratios (1025:1 here) even with very steep interface curvatures. The method is based on defining a distance function for each numerical cell, positive for one fluid, negative for the other fluid and zero for the fluids' interface. The magnitude of this distance function in each cell is equal to

the shortest distance from the fluid's interface. By advancing the distance function in time, the interface of the fluids can be tracked easily, hence the free surface of the waves is updated in every time step. More details about the level set method can be found in [31].

After locating the wave free surface by the level set method, the new hull position needs to be calculated. This can be achieved by using an immersed boundary method [32]. In the immersed boundary method, the solid body (hull here), is immersed in the numerical grid points, therefore there is no limitation regarding the solid motion plus no re-meshing technique needs to be adopted. In this method, initially the whole domain including the solid part is treated as fluid and the Navier-Stokes equations are solved throughout the whole domain. Then, additional constraints are imposed to the cells which are occupied by the solid. These constraints are rigid body motion for the solid cells, and no-penetration boundary condition on the solid-fluid interface. The rigid body constraint is imposed to solid cells by integrating the linear and angular momentum of the solid cells and defining a unique linear velocity and angular velocity for these cells. The equations to calculate the solid linear and angular velocities are based on the conservation of linear momentum and angular momentum of the solid cells and can be written as;

$$\begin{aligned} m_s \mathbf{u}_{s_{cg}} &= \int_\Omega C\mathbf{u}\rho \mathrm{d}\Omega \\ I_{s_{cg}}\omega_s &= \int_\Omega C(\mathbf{r}\times\mathbf{u})\rho \mathrm{d}\Omega. \end{aligned} \tag{3}$$

In Equation 3, m_s is the solid (hull) mass, $\mathbf{u}_{s_{cg}}$ is the solid velocity at the center of gravity, Ω is the numerical domain volume, C is a marker function to define whether a grid point is inside or outside the solid, $I_{s_{cg}}$ is the mass moment of inertia of the solid respect to the solid center of gravity, ω_s is the solid angular velocity, and finally r is a vector from the solid center of gravity to any grid point in the numerical domain. The linear and angular velocities from Equation 3 are used to update the solid cell velocities, resulting in a rigid motion for the solid.

The no-penetration boundary condition on the solid-fluid interface is imposed by forcing the velocities in the whole domain, including the cells through which the solid-fluid interface surface is passed, to be divergence free. Imposing each of rigid body and no-penetration constraints may slightly violate the other constraint, therefore a couple of iterations can be used to better satisfy both constraints. See [32] for more details about the immersed boundary method.

The described method is solved in a numerical domain shown in Figure 2. The platform is placed 4 wavelength from the wave generator and the grids are clustered around the platform (Figure 2a) and coarsened downstream to damp out the incoming waves (Figure 2b). Waves are generated from upstream end by defining an inflow-outflow boundary condition from linear Airy wave theory. As the wave propagates in the numerical domain, it becomes completely a nonlinear wave, since it is satisfying nonlinear boundary conditions (nonlinear free surface) and solved by the nonlinear equations (Navier-Stokes equations) [33]. The slip boundary condition is imposed on the other sides of the numerical domain except on the top which the air is allowed to go in and out to conserve the mass at each time

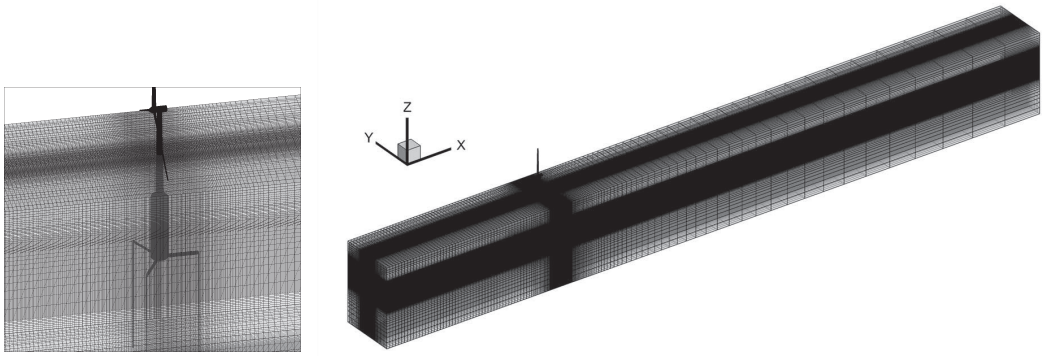

(a) (b)

Figure 2: Zoom in (a) and zoom out (b) view of discretized numerical domain used to model TLPWT in interaction with waves. $270 \times 85 \times 127$ number of grid points are used for baseline simulation.

step in the whole numerical domain

2.1.2. Structural Model

The TLPWT is considered as a two-body model. The first body consists of the rotor, nacelle and the tower rigidly connected together. The second body is the hull which is fully modeled in the fluid-structure interaction part. The connection between these two bodies are provided by a pin, rotational spring, and a rotational damper. The tendon effects are considered as external forces consists of a spring and a damper. The tendon forces reduce to zero in the slack condition.

The rotational spring stiffness at the connection point represents the tower first bending mode [34]. The reason for modeling the tower first bending mode is to investigate whether this mode can be excited by high order wave loads. In order to calculate this rotational spring coefficient, the tower potential energy due to a unit tip displacement in the first tower bending mode is calculated. The rotational spring coefficient should result in the same potential energy due to the same tower tip displacement. The rotational spring coefficient becomes;

$$k_{Tow} = C_{Cor} \frac{3EI_{CTow}}{L_{Tow}}, \tag{4}$$

where E is the tower modulus of elasticity, I_{CTow} is the tower cross section second moment of area, and L_{Tow} is the tower length. The tower first bending mode of the TLPWT can also be determined by a finite element model in the SR software. Therefore, a correction factor, C_{Cor} (0.81 here) is multiplied to the right hand side of Equation 4 to achieve the precise value. The tower structural damping ratio is 1% according to NREL 5 MW wind turbine reference manual [25]. Rayleigh damping model is applied to acquire approximately the desired damping ratio at the frequency of the tower first bending mode. This results in Rayleigh stiffness-proportional damping coefficients equals to 0.007 s and mass-proportional damping coefficient equal to zero [35].

After defining the tower rotational spring stiffness and damping coefficient, equations of motion for the first body (rotor-nacelle-tower) of the two-body model of TLPWT can be developed. A Lagrangian approach is chosen to develop the equations and the equations are linearized. The linearization can be justified because the pitch motions of the hull and tower are small due to the high stiffness of the TLP tendons and tower. Also, due to the high stiffness of TLPWT tendons in heave, the contribution of the heave coupling to the tower rotational motion is small enough to be neglected. This results in the following formula for the tower rotational angle. The TLPWT configuration, assuming a finite independent rotation of the hull and tower, is shown in Figure 3.

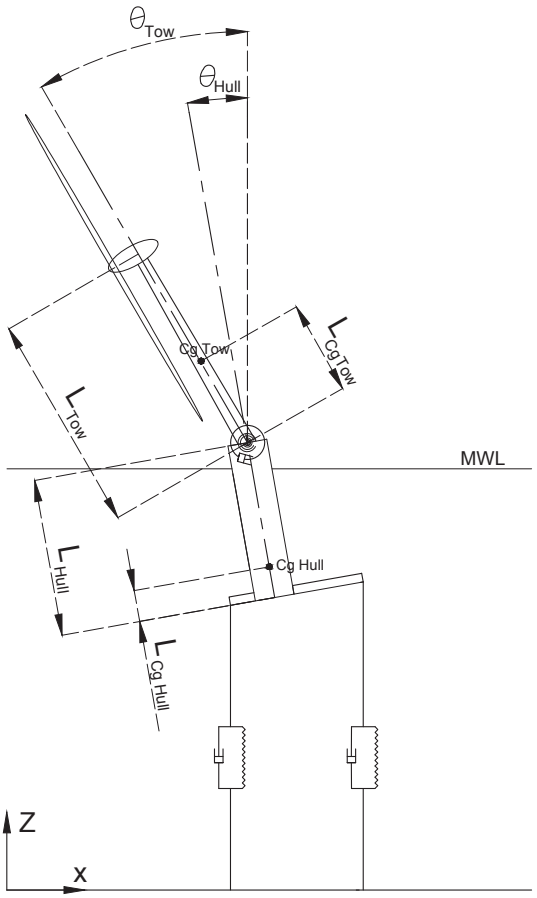

Figure 3: Parameters and models used to develop equation of motion for the tower. The angles are greatly exaggerated.

$$\Big(M_{Tow}L_{CgTow} + (M_{Nac} + M_{Rot})L_{Tow}\Big)\ddot{x}_{Hull} + ..$$
$$\Big(M_{Tow}L_{CgTow} + (M_{Nac} + M_{Rot})L_{Tow}\Big)(L_{Hull} - L_{CgHull})\ddot{\theta}_{Hull} + ...$$
$$\Big(Iyy_{Rot} + Iyy_{Tow} + (M_{Nac} + M_{Rot})L_{Tow}^2\Big)\ddot{\theta}_{Tow} + ...$$
$$C_{Tow}\dot{\theta}_{Tow} - C_{Tow}\dot{\theta}_{Hull} + ...$$

$$\Big(k_{Tow} - (M_{Nac} + M_{Rot})gL_{Tow} - M_{Tow}gL_{CgTow}\Big)\theta_{Tow} - k_{Tow}\theta_{Hull} = 0 \tag{5}$$

Equation 5 takes the hull kinematic values ($\ddot{x}_{Hull}, \ddot{\theta}_{Hull}, \dot{\theta}_{Hull}, \theta_{Hull}$) from the fluid-structure interaction part and updates the tower angle at the new time step.

The forces from the tendons along with the forces and moments from the tower will create a net force and a net moment on the hull. The net force and the moment are applied as a distributed force on each cell of the grid points occupied by the hull. This force creates **F** on the right hand side of the Equation 1.

In this approach, the hull kinematic values are imported from the fluid-structural part to the structural part, and the net force **F** is imported from the structural part to the fluid-structure part. Hence, information between the two parts is exchanged in each time step and the simulation is coupled. Few iterations can be performed in each time step to assure that the coupling terms (**F** and hull kinematic values) are fully converged, before marching to the next time step. However, in practice we have found it to be more computationally efficient to take smaller time steps and let each part use the information form previous time step of the other part and as a consequence iterations in every time step can be avoided.

Since in the presented numerical model the input of the fluid-structure interaction part from the structural part is a forcing term, the structural model presented here can be easily replaced with other structural models such as finite element models [11] or multi-body models with higher degrees of freedom [36]. In the current study the focus is on hydrodynamic analysis of TLPWT, therefore no wind load is applied. If desired, the wind forces can be applied to the rotor as function of time and the resultant force and moments will be treated as an additional external load [22].

2.2. Potential Flow Theory Based Model (SIMO-RIFLEX)

Simulations using SIMO-RIFLEX (SR) have also been carried out for comparison. This aero-hydro-servo-elastic simulation tool, developed by MARINTEK, has been used to study numerous types of floating wind turbines - both with an internal aerodynamic module and coupling to NREL's AeroDyn code [37, 35, 38]. SIMO [39] models the rigid body hydrodynamics of the hull while RIFLEX [40] includes the finite element solver, and flexible elements for the mooring lines or tendons, tower, shaft, and blades. The SIMO-RIFLEX simulation tool has been used and validated for various offshore structures [41, 42, 43, 44].

In the present simulations, the aerodynamic loading on the wind turbine is not included. The hull, rotor and nacelle are modeled as rigid bodies, while flexible beam elements are used to model the tower and tendons. First order potential flow forces (added mass, radiation damping, and excitation forces) and second-order sum-frequency quadratic transfer function wave loads are applied to the hull. The hydrodynamic coefficients and first and second order excitation forces are obtained in a panel code (WAMIT [45]) and subsequently used as input to SIMO. In addition to the potential flow forces, drag forces according to Morison's equation are applied to the center column ($C_D = 1.0$). Hydrodynamic forces are also applied on the tendons according to Morison's equation with $C_D = 0.7$ and $C_a = 1.0$. Based on the small tendon diameter and the fact that they are far from the free surface, the total

hydrodynamic forces on the tendons are negligible compared to the forces on the hull. The different structural and hydrodynamic models used in CFD and SR approaches are tabulated in Table 2.

Table 2: Numerical models, used in CFD based model and SIMO-RIFLEX (SR), to simulate a TLPWT.

TLPWT Components	CFD based Model	Potential flow theory based model (SR)
Hull	Rigid body	Rigid body
Tower	Rigid body, hinged at tower base +Rotational spring and damper	Flexible beam elements
Rotor & Nacelle	Rigid body	Rigid body
Tendons	Spring and damper	Flexible beam elements
Wave loads (hull)	Nonlinear (Navier-Stokes Eq.)	1st and 2nd order sum-frequency (potential flow theory) +Drag force (Morison equation)
Wave loads position	Instantaneous hull position	Mean hull position

3. Results

In this section, the TLPWT, described in section 2 (see Figure 1 and Table 1), is studied in detail. Initially, a grid sensitivity study is performed to get an insight about the effect of number of grid points on the TLPWT responses. Then, free decay tests are performed in different directions to assess the TLPWT natural frequencies. The responses of the TLPWT to regular waves is studied, and finally the effect of varying the wave height on the TLPWT response is investigated. All of the simulation results are compared with the SR software.

3.1. Grid Sensitivity Study

CFD models can handle very well nonlinear wave loads on offshore structures but usually require considerable computational time and cost. Therefore, assessing the required number of grid points is an important factor. In this section, a free heave decay test of the TLPWT is studied with various numbers of grid points. Since TLPWT has a high natural frequency in heave, even few seconds of heave decay simulation still contains number of response cycles that can give some insights about the effects of grid resolution on hydrodynamic parameters such as added mass and damping ratio.

An initial heave displacement from the hydrostatically stable position of the TLPWT is given and the results are plotted in Figure 4a. It can be seen that the frequency of the CFD results are converged for 10 million grid points and the result with 3 million grid points also gives very good predictions. It is interesting to note that even the results with 1 million grid points give an essentially accurate prediction for the platform heave frequency.

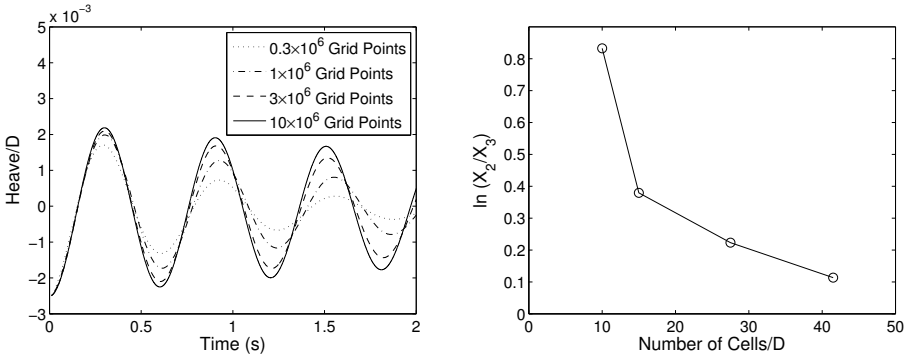

(a) (b)

Figure 4: (a) CFD model grid sensitivity study as a function of time for a heave decay test. (b) Effects of grid resolution on damping of heave response. Vertical axis; logarithmic ratio for second (X_2) and third (X_3) maximum heave responses in Figure 4a. Horizontal axis; number of cells used to resolve the TLPWT hull diameter, D.

Figure 4b, shows the effects of the number of grid points on the damping of the heave response. The vertical axis shows the logarithmic ratio of the second (X_2) to third (X_3) maximum peak in heave. The first peak response is not considered, since it might be affected by the initial heave displacement. It can be seen that precise prediction of heave damping requires more refined grids than heave frequency. In Figure 4b although the results are not fully converged, the convergence trend can be clearly seen. Simulations with finer grid points are desirable but avoided due to the very high computational cost.

From the above simulations, it can be concluded that parameters like added mass and hydrodynamic restoring stiffness governing the TLPWT natural frequencies can be modeled by using a relatively coarse grid. However, very accurate prediction of the damping coefficient requires a more refined grid points due to boundary layer contribution, and in this case, very small heave response. In the current study, wave frequency of interest is not close to the platform natural frequencies, hence the effects of viscous damping should be limited. Therefore, baseline number of grid points for the rest of the simulations was chosen to be 3 million grid points which results in very good accuracy in natural frequency and acceptable prediction for damping ratio, while allowing for reasonable simulation time.

3.2. Free Decay Tests

The surge and heave decay tests are performed by giving a finite displacement from the static equilibrium position. The results are plotted in Figure 5a and Figure 5b. A reasonable agreement in surge and heave natural frequencies can be seen. The CFD model predicts 0.117 rad/s and SR predicts 0.126 rad/s surge natural frequency. For the heave natural frequency, the CFD results predict 10.30 rad/s and the SR model 9.82 rad/s. Different models used to include the tendon forces (Table 2) can be the reason for the discrepancy in the surge and heave natural frequencies.

Damping in the surge decay test shows better agreement than the damping in heave. The heave response amplitude is on the order of 10^{-3} (normalized by the hull diameter) due to the high stiffness of TLPWT tendons and very

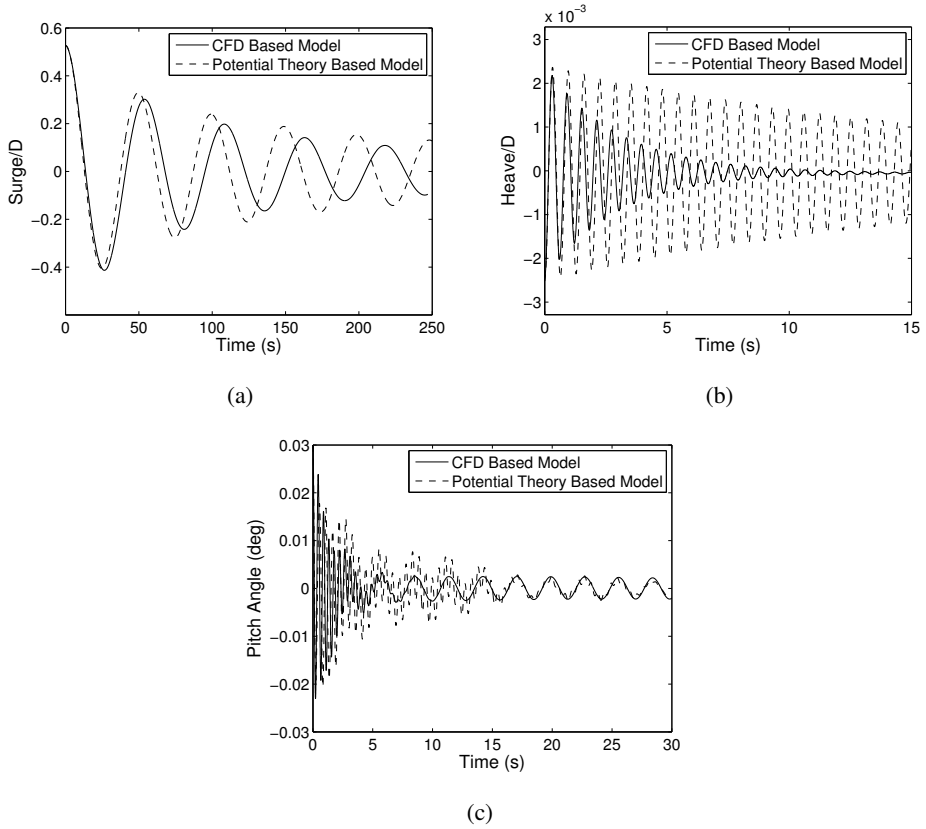

Figure 5: Surge, heave and pitch free decay tests of the TLPWT. The surge and heave responses are normalized by the hull diameter.

accurate modeling of radiational and viscous damping in this scale requires extremely fine grid points. However, heave damping should not greatly affect the TLPWT global response, because the heave natural frequency is very far from studied wave frequency and the typical ocean wave spectrum frequency range. Moreover, due to the large draft of the TLPWT hull, the wave loads on TLPWT in heave are limited. Some numerical analysis of TLPWTs shows promising results even by neglecting the heave motion [8].

Figure 5c shows the pitch decay responses of the TLPWT hull. An initial 0.03 *deg* pitch angle is given to the hull and tower of TLPWT (see Figure 3). Due to the high stiffness of the TLPWT tendons, a small initial pitch angle must be given, such that the tendons remain in tension. The TLPWT pitch response predicted by both the CFD and SR approaches is shown in Figure 5c. The CFD pitch decay test shows two natural frequencies at 2.22 rad/s and 14.28 rad/s. The lower natural frequency is primarily due to tower first bending mode natural frequency, while the higher natural frequency is more related to the TLPWT hull pitch motion and the stiff supporting tendons. The SR pitch decay test shows two dominant frequencies at 2.22 rad/s and 11.36 rad/s and some responses related to bending modes of tendons and second tower bending mode. In the CFD model, the tendons are modeled by external loads and the tower second bending mode is not considered. The main focus of the current investigation is related to the wave loads on the hull of the TLPWT and possible excitation of the first tower bending mode. Therefore, the simplification

of the tower and tendon structural models in the CFD approach should not greatly affect the interested results. The lower frequency damping in the pitch direction is a function of tower damping, given explicitly in Equation 5. The CFD model predicts more high-frequency damping than the SR approach probably due to the simplification of viscous damping in the SR model and/or due the numerical damping in the CFD model. As discussed in subsection 3.1, the damping effects on TLPWT global response for the regular waves outside of resonance frequency are limited.

3.3. TLP Response to a Regular Wave

In this part, the response of the TLPWT to a wave with 0.75 rad/s frequency and 7.7 m height is studied. 30 cells in wavelength are used to simulate propagated waves. Numerical damping leads to approximately 3.5% decrease in wave height per wavelength propagation, therefore higher amplitude wave is generated at the wave generator to reach the desired value at the platform position. In general, numerical damping of wave due to wave propagation varies depending on the wave steepness and number of cells resolving the wave.

The wave frequency was chosen such that the third-harmonic of the incoming wave frequency coincides with the first tower bending mode frequency. Assuming the maximum water's particle velocity as the representative velocity of the flow and TLP hull diameter as the representative length scale, the Reynolds number (Re) is equal to 4×10^7 and Keulegan-Carpenter number (KC) equal to 1.73, not accounting for the TLP hull relative velocity. If the TLP hull relative velocity becomes large, it may significantly affect the KC number [46]. However, the TLP maximum oscillating velocity, as it will be shown in the results, is less than 30% of the maximum water's particle velocity. Therefore, the Re and KC number will not vary significantly and the flow regime predicted here is accurate enough. For the considered simulation although the Reynolds number is high, due to low KC number there is not enough time for shedding of vortices behind the hull [47, 48]. Hence, the creation of strong vortices is not expected and using a turbulence model is not essential for the CFD simulations. Moreover, studied performed by Yu et al. [49] claimed that the presence of free surface may inhibit vortices near the wake of circular cylinder. Therefore, it is expected that shedding of vortices behind the TLPWT hull may occur at even higher KC numbers than the values reported for circular cylinder in the absence of free surface ($KC \simeq 4$ [48]).

It should be noted that, if the wave load analysis contains large KC and Re numbers, strong vortices may shed from the TLPWT hull. Therefore, accurate prediction of the flow field may require a turbulence model with a wall function to resolve properly the boundary layer. An example of using the current CFD approach with a turbulence model can be found in [50].

A snapshot of the numerical simulation, the related close-up view and the sectional velocity are shown in Figure 6. In the close-up view the small radiated waves around the hull can be seen. The sectional velocity is taken 5 meters below the mean water level to make sure it remains below the free surface. As expected, due to low KC number no shedding of vortices behind the hull can be seen. In this simulation, the ratio of the incoming wavelength to hull diameter is rather large, hence the diffraction of incoming wave by the hull is limited. Therefore, the flow field velocity at the front of cylinder (in this snapshot, right side of cylinder) contains the velocity component in x direction, while

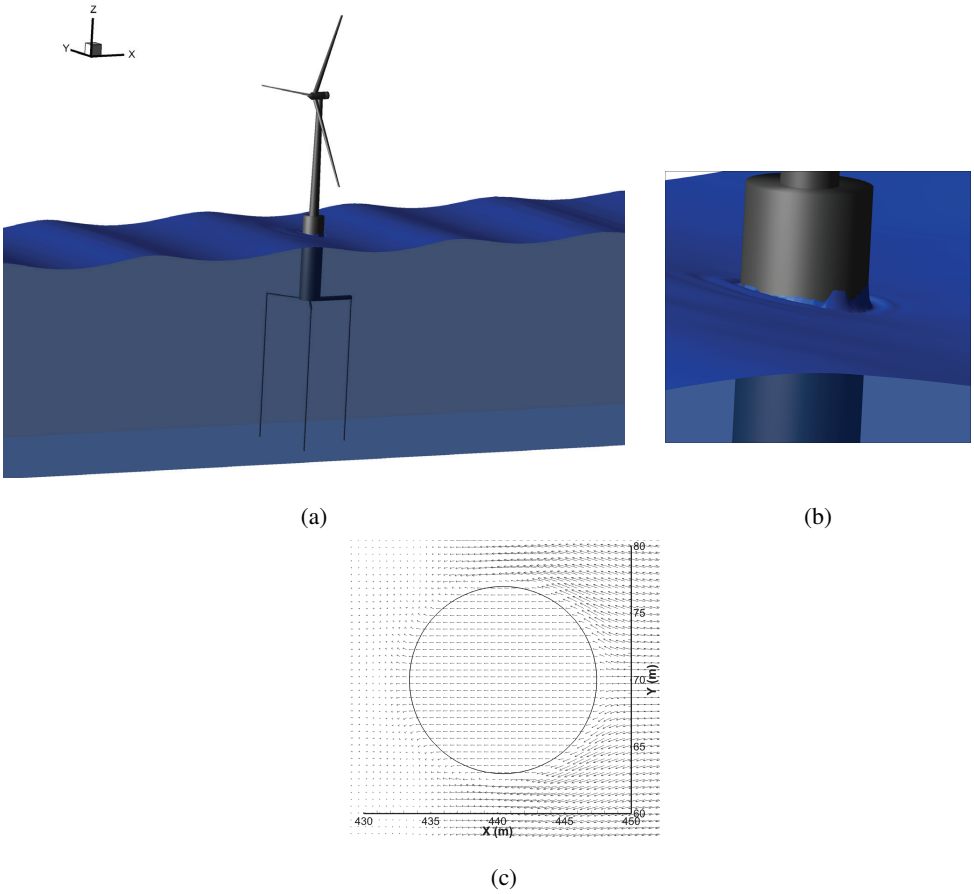

Figure 6: (a) Zoom out and (b) close up view of TLPWT. (c) Sectional velocity of the TLPWT hull 5 meter below the mean water level.

behind the cylinder (in this snapshot left side of cylinder) the velocity field shows small velocity components in x-y plane and contains larger values in z direction, which nearly follows the velocity field of undisturbed incoming wave.

Figure 7 shows the time domain and frequency domain amplitude of the incoming wave, simulated by the CFD and SR models. The wave gauge is placed 0.25λ upstream of the TLPWT. Although the wave gauge is placed close to the TLPWT, the wave diffracted by the TLPWT hull does not significantly affect the incoming waves due to the large ratio of the wavelength to the hull diameter ($\frac{\lambda}{D} = 7.8$). The waves generated by both models are in good agreement in amplitude and frequency. A small second-order wave component can be seen in the CFD frequency domain plot at $1.5\ rad/s$.

The surge response of the TLPWT, calculated by the CFD and SR models in the time domain and frequency domain, is shown in Figure 8. In the CFD model, there is a low frequency response at the TLPWT surge natural frequency, $0.115\ rad/s$. This low frequency response is due to the slow transient surge motion. The natural frequency of the TLPWT is very low and it takes very long time to completely damp out which makes the CFD computational cost prohibitively high. Fortunately, this low frequency response can be easily distinguished from the steady state

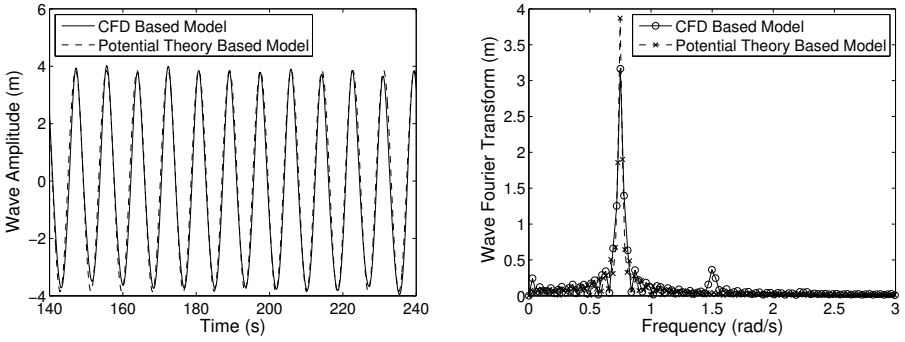

(a) (b)

Figure 7: Wave elevation measured 0.25λ upstream of TLPWT in the time and frequency domains.

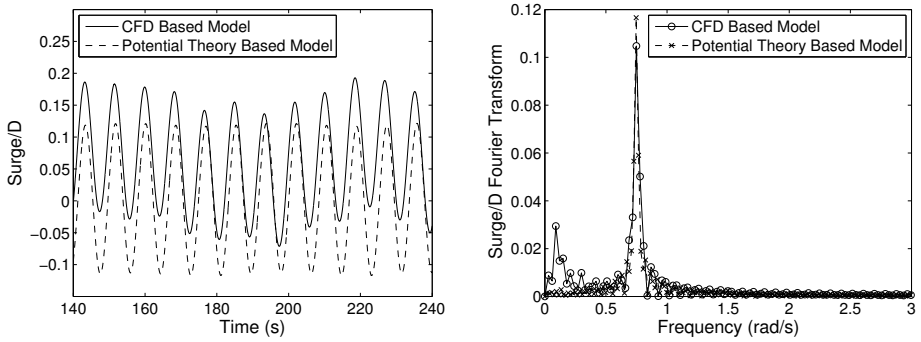

(a) (b)

Figure 8: The surge response of the TLPWT normalized by the hull diameter in the time and frequency domains. Larger mean surge can be seen in the CFD results.

response at the wave frequency ($0.75\,rad/s$) and coupling is not expected due to the large difference in the frequencies. In Figure 8a also a much larger mean surge in the CFD results ($S/D = 0.07$) can be seen compared to the SR model ($S/D = 0.0018$). This mean surge shifts the TLPWT downstream and heave response also will be affected. However, it will not vary significantly design driving parameters such as pitch motion, tendon forces and tower base moment because it only results in a new dynamic mean position. The response of both methods at the incoming wave frequency is in relatively good agreement and the difference between two approaches is within 8%.

The heave response of the TLPWT, calculated by the CFD and SR models in the time and frequency domains, is shown in Figure 9. In the CFD results, there is a low frequency response, a response at the wave frequency, and twice the wave frequency. The SR result shows a very small amplitude response at the wave frequency and a dominant response at twice the wave frequency. The heave motion of the TLPWT, as for the oil and gas TLPs, is mainly governed by the surge induced motion (set-down motion). The heave motion due to the heave force on the TLPWT is very small due to the high stiffness of TLPWT tendons. If the still water equilibrium position of the TLPWT is

used as the referenced point for measurements, both negative and positive surge motions result in a negative heave motion, which can be seen in both CFD and SR time domain results (Figure 9a). It can be seen that the main heave frequency response of the SR results is at twice the wave frequency, while according to the CFD results, the heave motion responds more with the wave frequency (Figure 9b). This difference is mainly due to the heave response induced by the mean surge motion which results in a lower heave position (negative heave) compared to the initial position (zero heave). When a wave crest reaches the TLPWT, after a quarter of the wave period the maximum surge response occurs and at the same time heave reaches to the maximum negative value. This can be seen in both the SR and the CFD results. The next quarter period, the TLPWT returns to the mean position, which is nearly zero heave for the SR model, while it is a negative value for the CFD model. A quarter period later, the TLPWT reaches the minimum surge position. Hence, according to the SR model the TLPWT again reaches to the maximum negative heave value and the heave cycle is completed. However, according to the CFD model, the heave value is not the same as half a period before because of the mean surge motion. According to Figure 9a the TLPWT after passing the zero heave value, reaches a position with smaller negative value. Therefore, the heave cycle is not completed yet in the CFD model and it takes another half wave period to be completed (in total one complete wave period).

Note that, in this simulation the amplitude of the mean surge motion is less than the peak to trough surge response at the wave frequency, therefore within a half period after the minimum heave is reached, the TLPWT will pass the zero heave position but will not reach exactly the same negative heave value. Hence the CFD results for the heave response show components of both the wave frequency and twice the wave frequency (Figure 9b). In the limit that the mean surge motion becomes larger than the peak to trough surge response at the wave frequency, the TLPWT will not reach the zero heave position at all, hence there is no heave response with twice the wave frequency. On the other hand, in the limit that the mean surge response becomes zero, within half a period the TLPWT passes the zero heave position and reaches exactly to the same negative heave value. Therefore in this case the CFD results, the same as the SR results, only will show heave response with twice the wave frequency.

Figure 9a also shows nonuniformity in the heave amplitude which is due to the undamped slow transient surge response of the TLPWT and can be observed in the frequency domain response as a small peak at 0.115 rad/s (surge natural frequency).

The pitch angle response of the TLPWT in the time domain and frequency domain is shown in Figure 10. The CFD results shows 15% lower response compared to the SR model. This difference can be due to the difference in the structural (tendons) or hydrodynamic load modeling. In the CFD model, the effects of hull motion for calculating hydrodynamic loads is take into account while in the SR model the hydrodynamic loads are applied at the hull mean position. This relative motion allows the hull to follow the wave and may cause lower moment on the hull. In the frequency domain response of the CFD model, there is a peak at 1.5 rad/s which is twice the wave frequency. The second-harmonic wave frequency response can also be seen in the SR model, although in this model the incoming wave only contains the linear wave (Figure 7b). Nonlinear models included in the SR software, such as integrating the drag force up to free surface as well as pitch coupling with other modes, can be the reason for the second-order pitch

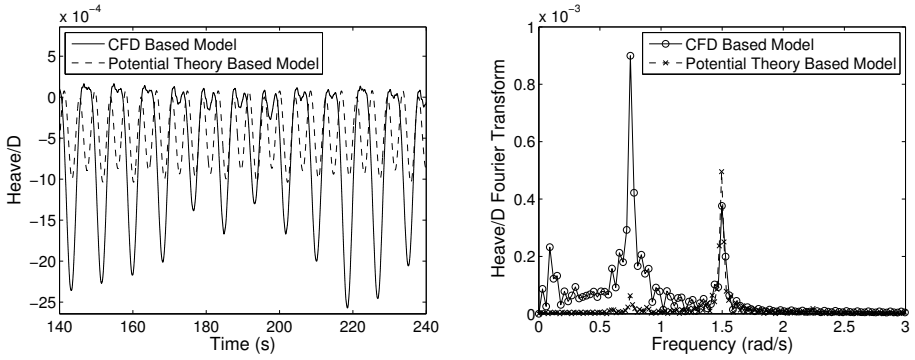

(a) (b)

Figure 9: The heave response of the TLPWT normalized by the hull diameter in time and frequency domain by CFD and potential flow theory based models. The difference is due to the heave response induced by the mean surge motion. The transient heave response induced by low frequency surge motion can also be seen in the CFD results.

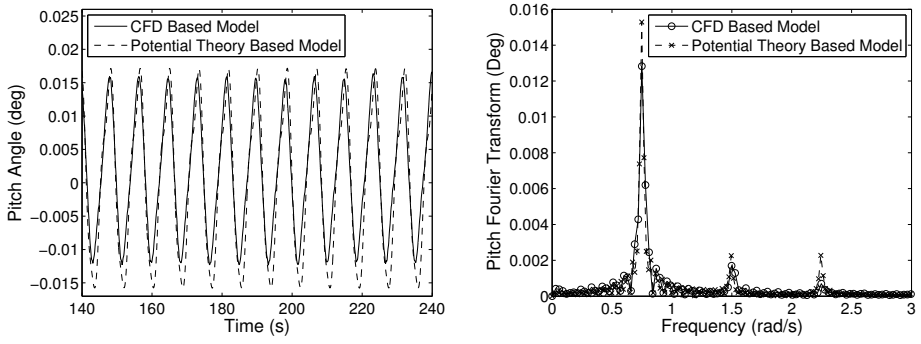

(a) (b)

Figure 10: The pitch response of the TLPWT in the time and frequency domains.

response. Also, in both models, there is a peak at 2.25 rad/s, which is third-harmonic wave frequency and coincides with the first tower bending mode. In the SR model, nonlinear models in the SR explained earlier, may result in a third-order harmonic load which will excite the tower natural frequency. The prediction of the third-harmonic pitch response amplitude is small. In the time domain CFD results, a mean positive pitch angle equal to 0.004 $degrees$ can also be seen which is most likely due to pitch moment caused by the mean wave force in surge direction.

The upstream and downstream tendon forces in the time domain and frequency domain are shown in Figure 11. Only one of the upstream tendon forces is shown since the other tendon force is identical (no-roll motion). The forces of the tendons are mainly function of the hull pitch response and the difference between tendon forces calculated by the CFD and SR models are within 6%. Comparing Figure 11 with Figure 10, it can be seen that, the second-harmonic and the third-harmonic forces are also following the hull pitch response. For the studied TLPWT, surge and heave do not contribute significantly to the TLPWT's tendon forces. The surge effects on the tendon forces are small, since

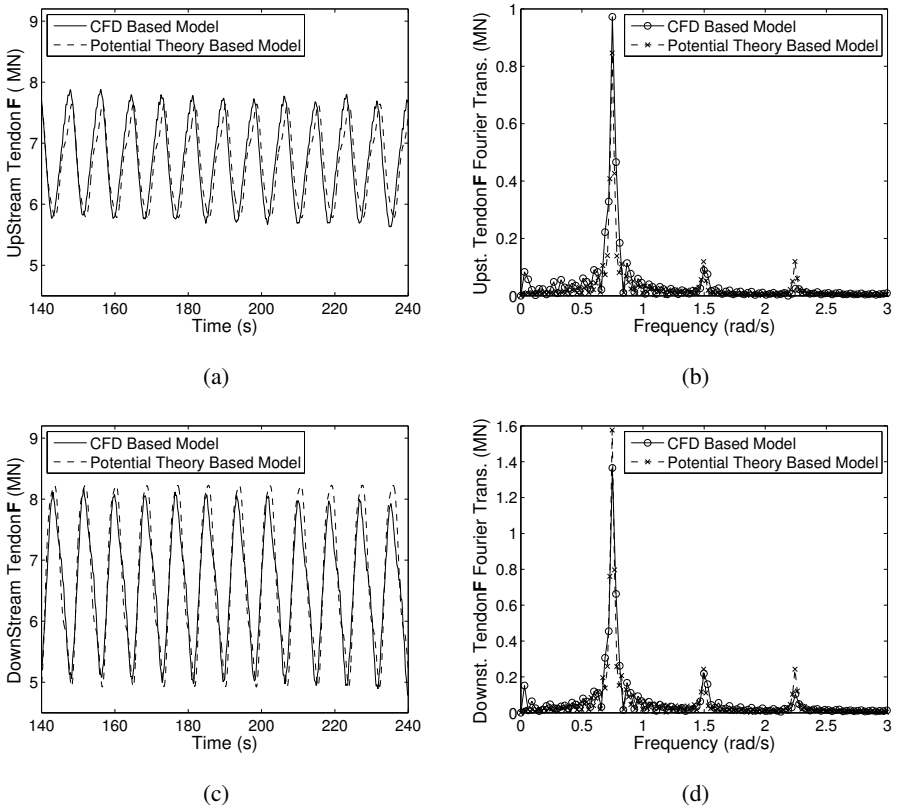

Figure 11: The upstream and downstream TLPWT tendon forces in the time and frequency domains.

the wave loads in the surge mainly results in rigid body set-down motion of the hull. The heave effects on the tendon forces is small as well, since the TLPWT heave response is very small. This is because the hull bottom is far from the free surface. Knowing that the wave forces reduce exponentially by the increase of distance from the free surface, the effective wave force applied to the hull bottom in the heave direction becomes very small.

The tower base bending moment in the time domain and frequency domain is shown in Figure 12. The tower base bending moment is mainly due to the surge motion of the nacelle and rotor masses on top of the tower, leading to a large moment on the base of the tower. The TLPWT pitch motion also contributes, but it is relatively small because of very limited TLPWT pitch angle (maximum 0.016 *deg* in the current simulation). The CFD results shows 19% higher moment compared to the SR model. Since the surge response is in good agreement, the discrepancy is most likely due to the difference in the tower modeling. In subsubsection 2.1.2, a correction factor (0.81) is multiplied to the representative rotational stiffness of the tower to obtain the desired first bending mode frequency. This correction factor results in reduction of the tower stiffness and can lead to over-prediction of tower base bending moment. In the CFD results, a second-harmonic response due to the second-harmonic component of pitch can be seen. In the frequency domain response by the SR model, a small peak at three times the wave frequency can be seen. Based on the CFD and SR results, the magnitude of the tower base bending moment due to the third-harmonic incoming wave

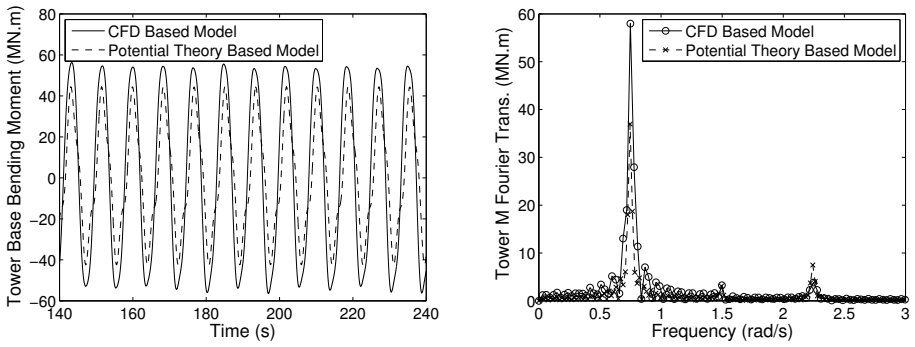

(a) (b)

Figure 12: The tower base bending moment of the TLPWT in the time domain and frequency domain.

is small compared to moment at the wave frequency, although the frequency coincides with tower first bending mode.

3.4. TLP Response to Different Wave Heights

The TLPWT is studied for wave heights 3.9, 6.0 and 7.7 m ($0.035 < H/\lambda < 0.071$) while keeping the wave frequency the same and the variation of responses are studied (Figure 13). As expected the differences between the CFD and SR results are smaller in the lower amplitude waves and larger in the larger ones. The surge shows a linear trend in both CFD and SR results with respect to wave amplitude. Frequency analysis of TLPWT surge response for wave height 7.7 m (Figure 8b) also shows very small contribution from the nonlinear terms. The pitch response shows excellent agreement in the smallest wave amplitude, while the difference becomes higher for the larger waves. The nonlinear trend can be due the higher order components of the incoming waves which can also be seen in frequency analysis of the TLPWT pitch response for wave height 7.7 m (Figure 10b). The CFD based results for maximum tendon forces, show better agreement for smallest wave and some differences in the larger ones. In the CFD results the upstream tendon forces are larger than SR results, while the downstream tendon forces are smaller. The difference should be due to the tendon forces induced by mean pitch response (Figure 10a). In the tower first bending moment results, there is a consistent difference between the CFD and SR model in all the wave heights. Since this difference also exists for the smallest wave in which nearly all the other responses are in good agreement, the difference is most likely due to modeling the tower as a single body in the CFD based approach.

3.5. Computational Time

In the CFD approach for hydrodynamic analysis of the TLPWT, the whole computational domain needs to be discretized, while in the potential flow theory approach, only the wet surface and the water free surface (second-order analysis) need to be resolved. Therefore, although CFD model gives more details about the flow field, it comes with considerably higher computational cost. For the baseline simulation described in subsection 3.3, details about computational cost of the two approaches are shown in Table 3.

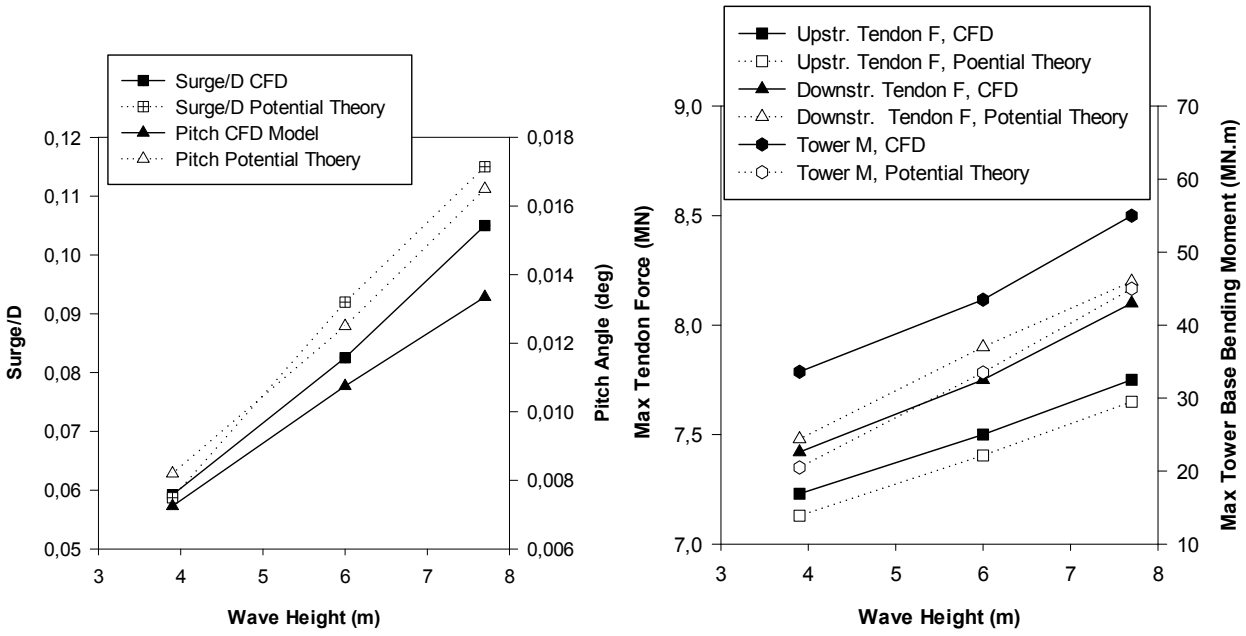

(a) (b)

Figure 13: Effects of wave amplitude on (a) TLPWT surge and pitch response amplitudes and (b) TLPWT maximum tendon forces and tower base bending moment.

4. Conclusions

A numerical approach based on Computational Fluid Dynamics (CFD) in combination with two-body structural model is developed. The developed model is then used in order to study wave induced responses of a Tension Leg Platform floating Wind Turbine (TLPWT) and to investigate resultant hydrodynamic loads on the tower and tendons. The results are compared with corresponding results based on a potential flow theory-finite element software, SIMO-RIFLEX (SR). The TLPWT dynamic behaviour is studied by performing a grid sensitivity study to assess the required number of grid points and free decay tests to determine its natural frequencies. The responses of the TLPWT to small and medium amplitude regular waves are studied and overall good agreement between both approaches is obtained.

Comparison of TLPWT responses performed by both approaches for incoming wave with 0.75 rad/s frequency and 7.7 m height are studied in detail. For this wave condition, the TLPWT surge shows a dominant response at the incoming wave frequency and good agreement between both approaches is observed. A higher mean surge is noted in the CFD based method. This can be due to better representation of nonlinear effects in the CFD based model, namely by applying the hydrodynamic force at the TLPWT instantaneous position and by integrating the hydrodynamic loads up to exact free surface. The higher mean surge in the CFD based model results in TLPWT mean position to be further downstream in surge and lower in heave. However, these differences do not considerably affect the TLPWT design driving parameters such as tendon forces and tower base moments, since it only affects the dynamic mean position of

Table 3: Comparing computational cost of the CFD and potential flow theory based models.

TLPWT model	CFD	Potential Flow Theory
Numerical grid points	3,000,000 cells	4868 panel cells
Physical Time	250 s	250 s
Time step	0.0016 s	0.01 s
Processor	1 CPU, Intel(R)E5-2687W @3.10GHz	1 CPU, Intel(R)X5660 @2.80GHz
Computational time	480 h (20 days)	WAMIT (hydrodynamic coef. and forces); 4 h SR (structural simulation); 1 minute

TLPWT.

Regarding the TLPWT hull pitch, more nonlinear components in response can be seen compared with surge and heave. This can be due to the variation of hull wet surface in time which results in nonlinear wave forces on the TLPWT. Since the free surface is far from the TLPWT center of gravity, relatively large nonlinear moment is induced on the hull.

Tendon forces are mainly governed by the TLPWT's pitch response, and the surge and heave responses do not highly contribute to the tendon forces. The surge contribution to the tendon forces is small since the surge response of the TLPWT mainly results in a rigid body set-down motion of TLPWT. The heave contribution to the tendon forces is small as well, because the hull bottom is far from the free surface and is not exposed to considerable wave loads.

In order to study the tower base bending moment in the CFD approach, the tower is modeled as a rigid body connected to the hull by a rotational spring and damper. The rotational spring stiffness is set such that the precise value for tower first bending mode frequency can be acquired. In the potential flow theory based model, however, finite element method is used to model the tower. Although different models are used, acceptable agreement between two approaches for the tower base bending moment is obtained. This agreement demonstrates that the simplified tower model used in the CFD based model can result in a reasonable estimation for tower base bending moment of TLPWT. In the current study the incoming wave frequency is set such that the third-harmonic wave frequency coincides with tower first bending mode frequency. However, for the studied wave heights a significant excitement of tower first bending mode is not observed. The very stiff tendons of TLPWT which results in linear hull and tower pitch motions, can explain the reason that the tower is not highly excited by the wave loads.

Finally, the effects of wave height variation on the TLPWT response is studied by both approaches. The difference between two approaches, as expected, is lower for the smaller waves and becomes larger as the wave height increases. The good agreement between the CFD and potential flow theory based models in small and medium amplitude waves gives confidence for further application of the proposed CFD-structural model for further application in hydrodynamic analysis of floating wind turbines.

5. Future work

In the current work, the authors investigate the accuracy of the developed CFD model by studying cases in which relatively good agreement between CFD and potential flow theory based results is expected. In future work, the focus will be one the cases where there may be larger discrepancies. The proposed CFD-structural model will be used to study a TLPWT for irregular waves in extreme ocean conditions in which the nonlinear effects such as ringing have high chance of occurrence and might significantly excite the tower first bending mode. The nonlinear wave induced responses determined by CFD method will be compared with predictions obtained by nonlinear potential flow theory based models such as nonlinear model developed by Faltinsen et al. [5].

References

[1] Corbetta G, Pineda I, Moccia J, Guillet J. The European offshore wind industry–key trends and statistics 2013. Uropean wind energy association. 2014.

[2] Walker R. Deep Water Oil Production System. In: SPE california regional meeting. 1968.

[3] Mercier JA, Leverette SJ, Bliault AL. Evaluation of Hutton TLP response to environmental loads. In: Offshore technology conference. 1982.

[4] Lonergan J, Fox F. Dynamic behaviour of models of tethered buoyant platforms. In: European offshore technology conference and exhibition. 1980.

[5] Faltinsen O, Newman J, Vinje T. Nonlinear wave loads on a slender vertical cylinder. J Fluid Mech 1995;289:179–98.

[6] Kumar A, Kim CH, et al. Ringing of heidrun tlp in high and steep random waves. Int J Offshore Polar Eng 2002;12(3):189–95.

[7] Musial W, Butterfield S, Boone A. Feasibility of floating platform systems for wind turbines. In: 23rd ASME wind energy symposium. 2004.

[8] Wayman E, Sclavounos P, Butterfield S, Jonkman J, Musial W. Coupled dynamic modeling of floating wind turbine systems. In: Offshore technology conference. 2006.

[9] Jonkman J, Matha D. Dynamics of offshore floating wind turbines analysis of three concepts. Wind Energy 2011;14(4):557–69.

[10] Sclavounos P, Lee S, DiPietro J, Potenza G, Caramuscio P, De Michele G. Floating offshore wind turbines: tension leg platform and taught leg buoy concepts supporting 3-5 MW wind turbines. In: European wind energy conference. 2010.

[11] Bachynski EE, Moan T. Design considerations for tension leg platform wind turbines. Mar Struct 2012;29(1):89–114.

[12] Roald L, Jonkman J, Robertson A, Chokani N. The effect of second-order hydrodynamics on floating offshore wind turbines. Energy Procedia 2013;35:253–64.

[13] Bae Y, Kim M. Rotor-floater-tether coupled dynamics including second-order sum–frequency wave loads for a mono-column-TLP-type FOWT (floating offshore wind turbine). Ocean Eng 2013;61:109–22.

[14] Bachynski EE, Moan T. Ringing loads on tension leg platform wind turbines. Ocean Eng 2014;84:237–48.

[15] Beyer F, Arnold M, Cheng PW. Analysis of Floating Offshore Wind Turbine Hydrodynamics Using Coupled CFD and Multibody Methods. In: 23rd international ocean and polar engineering conference. 2013.

[16] Jonkman B, Jonkman J. Documentation of updates to FAST, A2AD. and AeroDyn Released March 31, 2010, including the revised AeroDyn interface. Unpublished NREL technical report. 2010.

[17] Ren N, Li Y, Ou J. Coupled wind-wave time domain analysis of floating offshore wind turbine based on computational fluid dynamics method. J Renew Sustain Energy 2014;6(2):023106(1–20).

[18] Benitz MA, Schmidt DP, Lackner MA, Stewart GM, Jonkman J, Robertson A. Comparison of Hydrodynamic Load Predictions Between Reduced Order Engineering Models and Computational Fluid Dynamics for the OC4-DeepCwind Semi-Submersible. In: ASME 33rd international conference on ocean, offshore and arctic engineering. 2014.

[19] Liu C, Hu C. CFD Simulation of a Floating Wind Turbine Platform in Rough Sea Conditions. In: 24th international ocean and polar engineering conference. 2014.

[20] Hu C, Sueyoshi M, Kasuga F, Liu JC, Liu Y. Hydrodynamic analysis of a semi-submersible-type floating wind turbine. J Ocean Wind Energy 2014;1(4):202–8.

[21] Yabe T, Xiao F, Utsumi T. The constrained interpolation profile method for multiphase analysis. J Comput Phys 2001;169(2):556–93.

[22] Nematbakhsh A, Olinger DJ, Tryggvason G. A nonlinear computational model for floating wind turbines. J Fluid Eng 2013;135(12):121103(1–13).

[23] Nematbakhsh A, Olinger DJ, Tryggvason G. Nonlinear simulation of a spar buoy floating wind turbine under extreme ocean conditions. J Renew Sustain Energy 2014;6(3):033121(1–20).

[24] Nematbakhsh A, Bachynski EE, Gao Z, Moan T. Comparison of Wave-induced Response of a TLP Wind Turbine Obtained by CFD Method and Potential Theory. In: 24th international ocean and polar engineering conference. 2014.

[25] Jonkman JM, Butterfield S, Musial W, Scott G. Definition of a 5-MW reference wind turbine for offshore system development. National Renewable Energy Laboratory Golden, CO; 2009.

[26] Nematbakhsh A, Gao Z, Moan T. A CFD Based Numerical Wave Tank for Studying Wave Responses of Fixed and Floating Offshore Structures. To Appear. 2015.

[27] Harten A, Engquist B, Osher S, Chakravarthy SR. Uniformly high order accurate essentially non-oscillatory schemes, III. J Comput Phys 1987;71(2):231–303.

[28] Tryggvason G, Scardovelli R, Zaleski S. Direct numerical simulations of gas-liquid multiphase flows. Cambridge University Press Cambridge; 2011.

[29] Osher S, Sethian JA. Fronts propagating with curvature-dependent speed: algorithms based on Hamilton-Jacobi formulations. J Comput Phys 1988;79(1):12–49.

[30] Sussman M, Smereka P, Osher S. A level set approach for computing solutions to incompressible two-phase flow. J Comput Phys 1994;114(1):146–59.

[31] Osher S, Fedkiw R. Level set methods and dynamic implicit surfaces; vol. 153. Springer Science & Business Media; 2003.

[32] Curet OM, AlAli IK, MacIver MA, Patankar NA. A versatile implicit iterative approach for fully resolved simulation of self-propulsion. Computer Method Appl Mech Eng 2010;199(37):2417–24.

[33] Park JC, Kim MH, Miyata H. Fully non-linear free-surface simulations by a 3D viscous numerical wave tank. Int J Num Methods Fluid 1999;29(6):685–703.

[34] Rao SS, Yap FF. Mechanical vibrations; vol. 4. Addison-Wesley New York; 1995.

[35] Bachynski EE. Design and dynamic analysis of tension leg platform wind turbines. Ph.D. thesis; Norwegian University of Science and Technology; 2014.

[36] Wang L, Sweetman B. Multibody dynamics of floating wind turbines with large-amplitude motion. Appl Ocean Res 2013;43:1–10.

[37] Ormberg H, Bachynski EE. Global analysis of floating wind turbines: Code development, model sensitivity and benchmark study. In: 22nd international offshore and polar engineering conference. 2012.

[38] Bachynski EE, Kvittem MI, Luan C, Moan T. Wind-wave misalignment effects on floating wind turbines: motions and tower load effects. J Offshore Mech Arc Eng 2014;136:041902(1–12).

[39] SIMO users manual. MARINTEK Inc. Otto Nielsens veg 10, Trondheim, NO-7491 Norway; 2011.

[40] RIFLEX users manual. MARINTEK Inc. Otto Nielsens veg 10, Trondheim, NO-7491 Norway; 2011.

[41] Krokstad JR, Stansberg CT, Nestegard A, Marthinsen T. A new nonslender ringing load approach verified against experiments. J Offshore Mech Arc Eng 1998;120(1):20–9.

[42] Ormberg H, Stansberg CT, Yttervik R, Kleiven G. Integrated vessel motion and mooring analysis applied in hybrid model testing. In: 9th International Offshore and Polar Engineering Conference. 1999.

[43] Stansberg C, Yttervik R, Oritsland O, Kleiven G. Hydrodynamic model test verification of a floating platform system in 3000 m water depth.

In: Offshore technology conference. 2000.

[44] Kendon TE, Oritsland O, Baarholm RJ, Karlsen SI, Stansberg CT, Rossi RR, et al. Ultra-deepwater model testing of a semisubmersible and hybrid verification. In: 27th international conference on offshore mechanics and arctic engineering. 2008.

[45] WAMIT . WAMIT 7.0 User manual. WAMIT, Inc. 822 Boylston St. Suite 202 Chestnut Hill, MA 02467-2504 USA; 2012.

[46] Downes K, Rockwell D. Oscillations of a vertical elastically mounted cylinder in a wave: imaging of vortex patterns. J fluid struct 2003;17(7):1017–33.

[47] Sarpkaya T. Force on a circular cylinder in viscous oscillatory flow at low Keulegan-Carpenter numbers. J Fluid Mech 1986;165:61–71.

[48] Guilmineau E, Queutey P. A numerical simulation of vortex shedding from an oscillating circular cylinder. J Fluid Struct 2002;16(6):773–94.

[49] Yu G, Avital E, Williams J. Large eddy simulation of flow past free surface piercing circular cylinders. J Fluid Eng 2008;130(10):101304(1–9).

[50] Yang J, Stern F. Sharp interface immersed-boundary/level-set method for wave–body interactions. Journal of Computational Physics 2009;228(17):6590–616.